Organic & Biomolecular Chemistry

Cite this: *Org. Biomol. Chem.*, 2012, **10**, 2453

www.rsc.org/obc

PAPER

Studies on the conformational flexibility of α-L-rhamnose-containing oligosaccharides using ^{13}C-site-specific labeling, NMR spectroscopy and molecular simulations: implications for the three-dimensional structure of bacterial rhamnan polysaccharides

K. Hanna M. Jonsson, Elin Säwén and Göran Widmalm*

Received 15th November 2011, Accepted 6th January 2012
DOI: 10.1039/c2ob06924e

Bacterial polysaccharides are comprised of a variety of monosaccharides, L-rhamnose (6-deoxy-L-mannose) being one of them. This sugar is often part of α-(1 → 2)- and/or α-(1 → 3)-linkages and we have therefore studied the disaccharide α-L-Rha*p*-(1 → 2)-α-L-Rha*p*-OMe to obtain information on conformational preferences at this glycosidic linkage. The target disaccharide was synthesized with ^{13}C site-specific labeling at C1′ and at C2′, *i.e.*, in the terminal group. 2D ^{1}H,^{13}C-HSQC-HECADE and ^{1}H,^{13}C-J-HMBC NMR experiments, 1D ^{13}C and ^{1}H NMR spectra together with total line-shape analysis were used to extract conformationally dependent hetero- and homonuclear spin–spin coupling constants. This resulted in the determination of $^{2}J_{C2',H1'}$, $^{3}J_{C1',C1}$, $^{3}J_{C1',C3}$, $^{3}J_{C2',C2}$, $^{2}J_{C1',C2}$, $^{1}J_{C1',C2'}$, and $^{1}J_{C1',H1'}$. These data together with previously determined J_{CH} and ^{1}H,^{1}H NOEs result in fourteen conformationally dependent NMR parameters that are available for analysis of glycosidic linkage flexibility and conformational preferences. A 100 ns molecular dynamics (MD) simulation of the disaccharide with explicit water molecules as solvent showed a major conformational state at $\phi_H \approx 40°$ and $\psi_H \approx -35°$, consistent with experimental NMR data. In addition, MD simulations were carried out also for α-L-Rha*p*-(1 → 3)-α-L-Rha*p*-OMe and a rhamnan hexasaccharide. The gathered information on the oligosaccharides was used to address conformational preferences for a larger structure, a 2- and 3-linked nonasaccharide, with implications for the 3D structure of rhamnan polysaccharides, which should be regarded as flexible polymers.

Introduction

In carbohydrate structures from humans the number of different monosaccharides is quite limited; typically seven different sugars are present in glycoproteins and glycolipids.[1] Constituents of polysaccharides in man add a few more monosaccharides to the repertoire. In bacteria, however, more than 100 different monosaccharide components have been found.[2] One of them, L-rhamnose (6-deoxy-L-mannose) is present as a major constituent of the O-antigen polysaccharides from *Shigella flexneri*[3,4] and is the sole monosaccharide in the repeating unit of an O-antigen from a *Klebsiella pneumoniae* strain.[5] It is the constituent sugar of the O-glycan part of the S-layer glycoprotein in *Geobacillus stearothermophilus*[6] and the backbone of the O-specific polysaccharide from the lipopolysaccharide of *Aeromonas bestiarum* strain 207 is comprised of L-rhamnose residues.[7] Furthermore, it is often a constituent of the O-antigen of lipopolysaccharides (LPS) from Gram-negative bacteria that are associated with plants.[8] The LPS then act as part of the barrier that protects the bacteria from plant-derived antimicrobial substances. These polysaccharide structures are conversely recognized as non-self by the plant innate immune system and coiled polysaccharide structures may be of importance in interactions between bacteria and plants.

In many of the above mentioned polysaccharides L-rhamnose residues are joined by α-(1 → 2)- and/or α-(1 → 3)-linkages and conformational analysis of polysaccharides or oligosaccharides being models for these polymers is often based on measurements of the nuclear Overhauser effect (NOE) between protons in different sugar residues.[9–12] The experimental NMR data are subsequently analyzed in the light of a molecular simulation which employs a certain molecular mechanics force field.[13,14] Additional information on conformational preferences in rhamnose-containing oligosaccharides have been obtained from transglycosidic heteronuclear coupling constants.[15,16] These $^{3}J_{CH}$ are important and to date a large number of NMR experiments have been developed to this end.[17–26] The long-range heteronuclear coupling constants report on conformational averaging in a different way compared to the NOEs which are inversely

Department of Organic Chemistry, Arrhenius Laboratory, Stockholm University, S-106 91 Stockholm, Sweden. E-mail: gw@organ.su.se

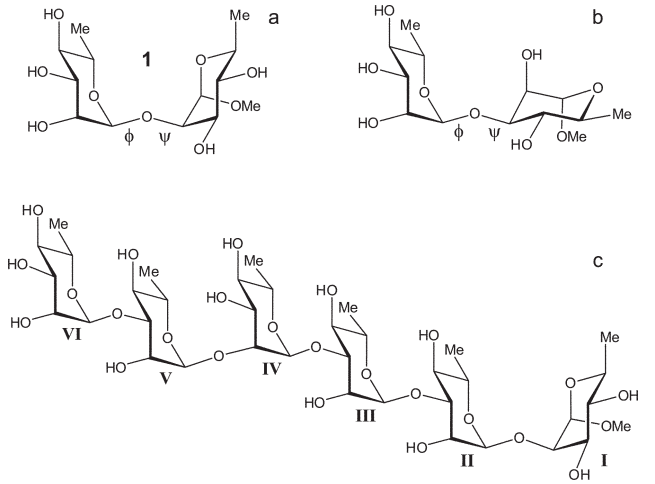

Fig. 1 Schematic of (a) α-L-Rha*p*-(1 → 2)-α-L-Rha*p*-OMe and (b) α-L-Rha*p*-(1 → 3)-α-L-Rha*p*-OMe with torsion angles ϕ and ψ indicated and (c) α-L-Rha*p*-(1 → 3)-α-L-Rha*p*-(1 → 2)-α-L-Rha*p*-(1 → 3)-α-L-Rha*p*-(1 → 3)-α-L-Rha*p*-(1 → 2)-α-L-Rha*p*-OMe with sugar residues I–VI indicated.

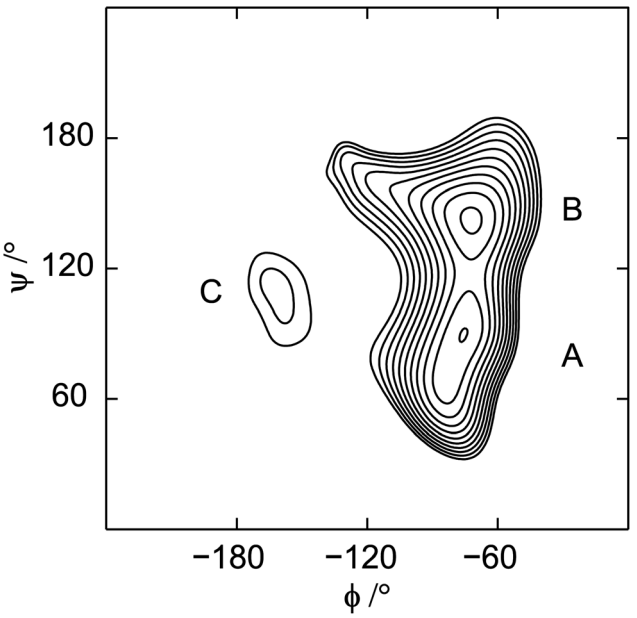

Fig. 2 Ramachandran map of α-L-Rha*p*-(1 → 2)-α-L-Rha*p*-OMe using the PARM22/SU01 force field, a dielectric constant of 3, and a grid size of 15°. Contour lines are drawn at 0.3 kcal mol^{-1} increments above the global energy minimum. Low energy conformational states are denoted by A, B and C.

proportional to a distance averaging according to r_{ij}^{-6}, where r_{ij} is the internuclear distance between protons i and j. However, the $^3J_{CH}$ have to be analyzed by a Karplus-type relationship in which several solutions to the conformational averaging process may be possible for a given coupling constant. Furthermore, the Karplus-curves need to be adequately parameterized for the coupling pathway under study.

The disaccharide α-L-Rha*p*-(1 → 2)-α-L-Rha*p*-OMe (Fig. 1), also referred to as R2R, is a model for the constituent disaccharide in these polysaccharides and has been studied previously using NMR spectroscopy, molecular mechanics calculations and molecular simulations.[27–29] To date four interresidue ^{1}H,^{1}H-NOEs, the two transglycosidic $^3J_{CH}$ coupling constants as well as residual dipolar coupling data have been measured.[30] To generate additional experimental NMR data for its conformational analysis we have now synthesized two isotopologues of R2R in which the C1′ and the C2′ atoms in the terminal sugar residue are ^{13}C site-specifically labeled. This labeling scheme facilitates determination of conformationally dependent homonuclear $^3J_{CC}$ coupling constants related to the glycosidic torsion angles ϕ and ψ. The determination of heteronuclear coupling constants were carried out by two-dimensional J-HMBC and HSQC-HECADE NMR experiments using either natural abundance or site-specifically ^{13}C-labeled disaccharides. In addition, $^nJ_{CH}$ were obtained by total-lineshape analysis NMR spectral simulations of the site-specifically ^{13}C-labeled R2R molecules. The establishment of seven conformationally dependent coupling constants will be described in this study. Furthermore, molecular mechanics methodology and molecular dynamics (MD) simulations are used to assess conformational flexibility and population distributions in R2R. Comparisons of data from NMR experiments to those obtained by the MD simulation ascertain whether the molecular description of R2R is suitable as a basis for delineating oligo- and polysaccharide conformation and dynamics. Additionally, MD simulations were carried out for α-L-Rha*p*-(1 → 3)-α-L-Rha*p*-OMe and a hexasaccharide and the simulation results were used to address conformational preferences of a nonasaccharide, the results of which have implications for the 3D structure of rhamnan polysaccharides.

Results and discussion

The synthesis pathway to the three target molecules, α-L-Rha*p*-(1 → 2)-α-L-Rha*p*-OMe (**1**), α-L-[1′-^{13}C]Rha*p*-(1 → 2)-α-L-Rha*p*-OMe (**1-*c*1′**) and α-L-[2′-^{13}C]Rha*p*-(1 → 2)-α-L-Rha*p*-OMe (**1-*c*2′**), was executed as in the previously published synthesis of **1**[31] with one exception: the target molecules were to be protected solely with benzoyl groups to carry out the deprotection in one step only. The donor, 2,3,4-tri-*O*-benzoyl-α-L-rhamnopyranosyl bromide (**2**), and its ^{13}C-isotopologues, were prepared by an initial per-benzoylation and then treated with HBr in HOAc, thereby forming the α-bromide product.[32] The acceptor, methyl 3,4-di-*O*-benzoyl-α-L-rhamnopyranoside (**3**), was synthesized from methyl 4-*O*-benzoyl-2,3-*O*-isopropylidene-α-L-rhamnnopyranoside[33] using the procedure described by Norberg *et al.*[34] The glycosylation reaction to form the protected disaccharide **4** was performed at low temperature with acceptor in excess using silver triflate as a promotor.[35] Finally, the fully benzoylated disaccharide **4** was deprotected according to standard procedures. The target molecules **1**, **1-*c*1′** and **1-*c*2′** were obtained in 54, 60 and 66% yield, respectively, starting from L-rhamnose or its isotopologues.

The conformational space available to R2R may be investigated by a Ramachandran map in which all degrees of freedom are relaxed except for the glycosidic torsion angles ϕ and ψ (Fig. 2). There are two low energy regions denoted A and B where the conformation at the ϕ torsion angle is governed by the *exo*-anomeric effect.[36] An additional region, labeled C, known as the non-exo-anomeric conformation can be identified. This

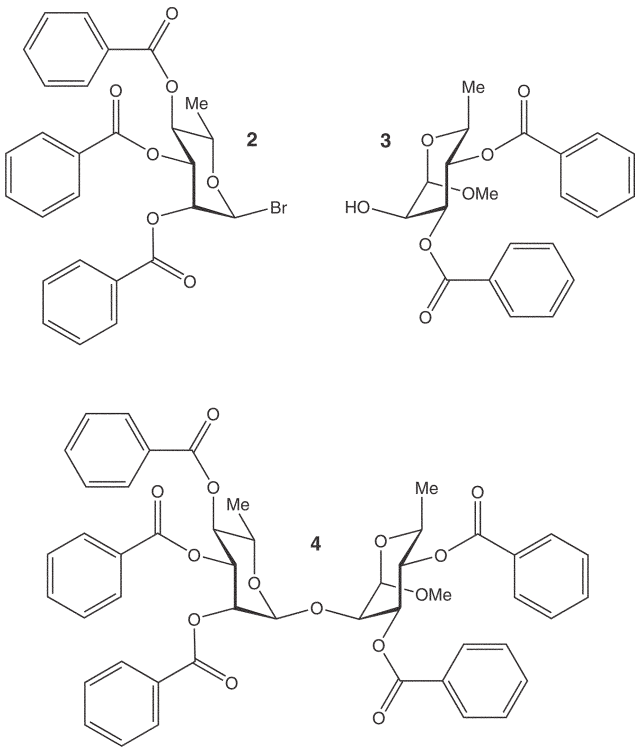

Ramachandran map, created using the CHARMM SU/01 force field modified for carbohydrates,[37] is similar to that previously described[14] employing an MM3 molecular mechanics force field. However, the simplified HSEA force field[36] results in a B-conformer at the global energy minimum.[38] A better description of the indicated conformational equilibrium will be possible if additional experimental data are utilized, *e.g.* the hitherto lacking transglycosidic $^{3}J_{CC}$ coupling constants.

The site-specific ^{13}C-labeling, at C2′ and at C1′, facilitates torsion angle information to be obtained *via* Karplus-type relationships for ϕ and ψ, respectively. At the ψ torsion angle three three-bond coupling constants are available if determined, *viz.*, $^{3}J_{C1',H2}$, $^{3}J_{C1',C1}$ and $^{3}J_{C1',C3}$ (Fig. 3). The heteronuclear coupling constant was previously determined using a one-dimensional long-range (1DLR) experiment.[39] Additional determination of this heteronuclear *J*-coupling is herein carried out by alternative methods. The two carbon-13 homonuclear coupling constants have so far not been determined for R2R. At the ϕ torsion angle three conformationally dependent coupling constants are available; $^{3}J_{C2,H1'}$ was estimated in a previous study and $^{3}J_{C2',C2}$ determined herein. The L-[2-^{13}C]Rha*p*-labeling aids accurate determination of $^{2}J_{C2',H1'}$ by different techniques and information on this coupling constant may be useful since Klepach *et al.*[40] recently showed that this heteronuclear coupling constant has a conformational dependence on the ϕ torsion angle. Three coupling constant relationships are thus accessible also for this torsion angle, *viz.*, $^{2}J_{C2',H1'}$, $^{3}J_{C2',C2}$ and $^{3}J_{C2,H1'}$. The transglycosidic homonuclear coupling constants were readily determined in ^{13}C-labeled R2R isotopologues from resolution enhanced 1D proton-decoupled ^{13}C NMR spectra as shown in Fig. 4. The $^{3}J_{CC}$ coupling constants are compiled in

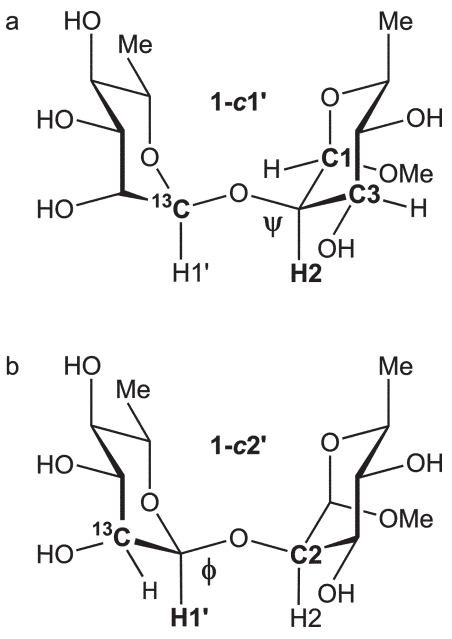

Fig. 3 Schematic of (a) [1′-^{13}C]-R2R site-specifically labeled with carbon-13 for measurement of $^{3}J_{CC}$ and $^{3}J_{CH}$ related to the torsion angle ψ; (b) [2′-^{13}C]-R2R site-specifically labeled with carbon-13 for measurement of $^{3}J_{CC}$ and $^{2}J_{CH}$ related to the torsion angle ϕ. Pertinent proton and carbon atoms are highlighted in bold characters.

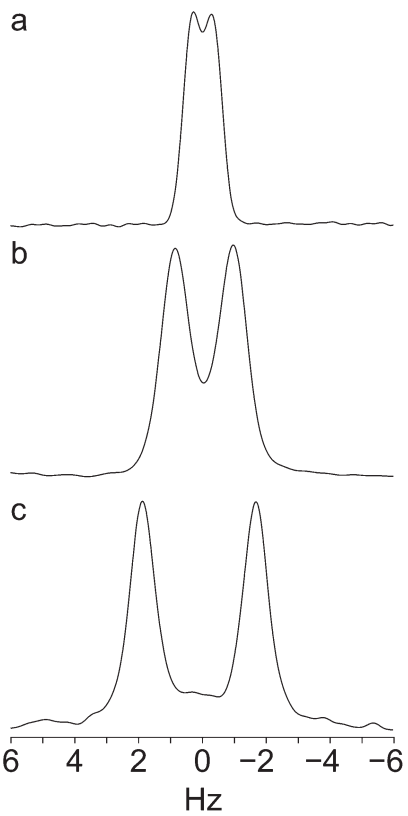

Fig. 4 Selected resonances from the ^{13}C NMR spectra of (a) [1′-^{13}C]-R2R showing $^{3}J_{C1',C1}$ = 0.7 Hz; (b) [1′-^{13}C]-R2R showing $^{3}J_{C1',C3}$ = 1.9 Hz; (c) [2′-^{13}C]-R2R showing $^{3}J_{C2',C2}$ = 3.6 Hz.

Table 1 Two- and three-bond $^{n}J_{CH}$ (Hz) in R2R from 1DLR, J-HMBC, and HSQC-HECADE experiments, total line-shape analysis and $^{3}J_{CC}$ (Hz) from ^{13}C NMR experiments. Pertinent torsion angles are indicated

Coupling constant	1DLR[a]	J-HMBC	HSQC-HECADE	Spin simulation	^{13}C	Compound	Torsion angle
$^{3}J_{H1',C2}$	4.2, 4.3	4.12 (0.20)[b]				**1**	ϕ_H
$^{3}J_{C2',C2}$					3.6	**1-*c*2′**	$\phi_{C2'}$
$^{2}J_{C2',H1'}$			–2.2	–2.33		**1-*c*2′**	ϕ_H
$^{3}J_{C1',H2}$	4.7, 4.8	4.52 (0.07)		4.59		**1/1-*c*1′**	ψ_H
$^{3}J_{C1',C1}$					0.7	**1-*c*1′**	ψ_{C1}
$^{3}J_{C1',C3}$					1.9	**1-*c*1′**	ψ_{C3}

[a] From ref. 29. [b] Standard deviations are given in parenthesis.

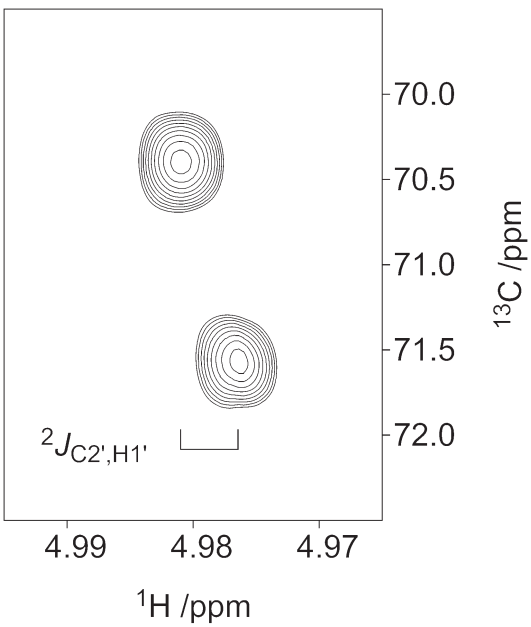

Fig. 5 Selected part from the $^{1}H,^{13}C$-HSQC-HECADE NMR spectrum of [2′-^{13}C]-R2R demonstrating the tilting of the cross-peak and the $^{2}J_{C2',H1'}$ coupling constant of −2.2 Hz measured in the F_2 dimension.

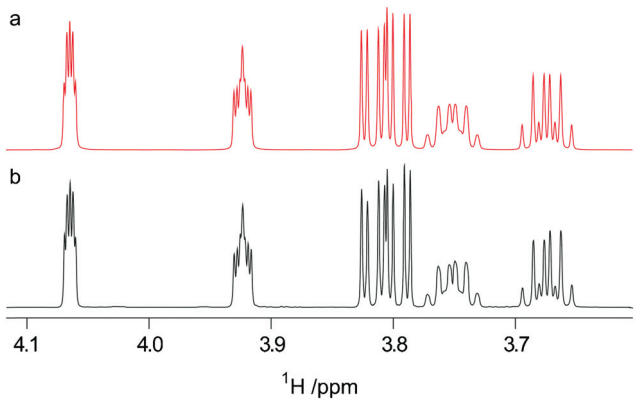

Fig. 6 ^{1}H NMR analysis at 700 MHz of [1′-^{13}C]-R2R: (a) simulated spectrum by total-lineshape analysis using the PERCH NMR software to obtain, in particular, $^{n}J_{CH}$ coupling constants; (b) experimental spectrum.

Table 1. The transglycosidic $^{2}J_{COC}$ coupling constant may also reveal some conformational information,[41] *i.e.*, in respect to the ϕ torsion angle, and from the ^{13}C NMR spectrum of **1-*c*1′** it could be established. The two-bond homonuclear coupling constant $^{2}J_{C1',C2} = -1.9$ Hz in R2R, assuming that the sign of the two-bond coupling is negative.[42]

Heteronuclear coupling constants over two and three bonds were measured by two different 2D NMR experiments, *viz.*, the $^{1}H,^{13}C$-HSQC-HECADE experiment[43,44] that utilizes $^{1}H,^{1}H$-TOSCY transfer and the $^{2}J_{CH}$ and/or $^{3}J_{CH}$ are determined from cross-peak separations in the F_2-dimension; the J-HMBC experiment[45] employs a scaling factor κ in the F_1 dimension and for sufficiently large values of κ the $^{n}J_{CH}$ couplings are readily determined from the cross-peak separation. The HSQC-HECADE experiment employed with a 30 ms isotropic mixing period resulted in a small tilt of the cross-peaks from $^{2}J_{C2',H1'}$ corresponding to a negative coupling constant as shown in Fig. 5. The the J-HMBC experiment was used to measure the transglycosidic $^{3}J_{C1',H2}$ and $^{3}J_{C2,H1'}$ coupling constants and the results are compiled in Table 1.

An alternative approach to obtain the heteronuclear coupling constants is to carry out a total line-shape analysis[46] of the ^{1}H NMR spectra of the site-specifically ^{13}C-labeled compounds. The ^{1}H and ^{13}C NMR chemical shifts in **1** were assigned at 310 K using standard 2D NMR experiments[47] and ^{1}H chemical shifts and $^{3}J_{HH}$ were subsequently refined using the NMR spin-simulation software PERCH. Further analysis was the performed for **1-*c*1′** (Fig. 6) and **1-*c*2′** to obtain $^{n}J_{C,H}$ (Table 2). There are in addition three ^{1}J coupling constants that may contribute information on conformational preferences through their torsion angle dependence, *viz.*, $^{1}J_{C1',C2'}$, $^{1}J_{C1',H1'}$ and $^{1}J_{Cn,Hn}$, where *n* is the substitution position.[48,49] In R2R $^{1}J_{C1',C2'} = 47.5$ Hz, determined from **1-*c*1′** and **1-*c*2′**. In the present study $^{1}J_{C1',H1'} = 170.49$ Hz from the total line-shape analysis of **1-*c*1′** compared to the value of 170.85 Hz obtained from *J*-modulated constant-time HSQC experiments of **1**,[30] which also resulted in $^{1}J_{C2,H2} = 149.20$ Hz. The agreement between different NMR approaches is very good and we have thus herein obtained and compiled eight coupling constants related to the conformationally dependent torsion angles ϕ and ψ in addition to the previously reported two $^{3}J_{CH}$ and four NOEs, that can be used in the conformational analysis of R2R. Thus, no less than fourteen NMR parameters related to a single glycosidic linkage are available in the conformational analysis of the molecule in isotropic solution, *i.e.*, it is not perturbed to any extent by an alignment medium which may influence the distribution of conformational states such when

Table 2 ^{1}H and ^{13}C NMR chemical shifts of **1** in D_2O at 37 °C. The heteronuclear coupling constants were obtained using **1-*c*1′** and **1-*c*2′**. The ^{1}H NMR chemical shifts and coupling constants were refined using the PERCH NMR software. Coupling constants, $^{3}J_{HH}$ in parentheses, $^{1}J_{CH}$ in braces, $^{n}J_{C1',H}$ in angle brackets, and $^{n}J_{C2',H}$ in square brackets, are given in Hz

Sugar residue	1	2	3	4	5	6	OMe
α-L-Rha*p*(1 →	4.962	4.065	3.796	3.451	3.751	1.276	
	(1.85)	(3.40)	(9.77)	(9.59)	(6.31)		
	{170.49}	⟨1.41⟩			⟨1.19⟩		
		{149.90}	[1.27]	[0.84]	[−0.15]		
→ 2)-α-L-Rha*p*-OMe	103.01	70.89	70.91	72.85	69.94	17.43	
	4.787	3.923	3.816	3.464	3.673	1.306	3.401
	(1.78)	(3.42)	(9.79)	(9.56)	(6.27)		
	100.42	79.30	70.86	72.99	69.40	17.46	55.71

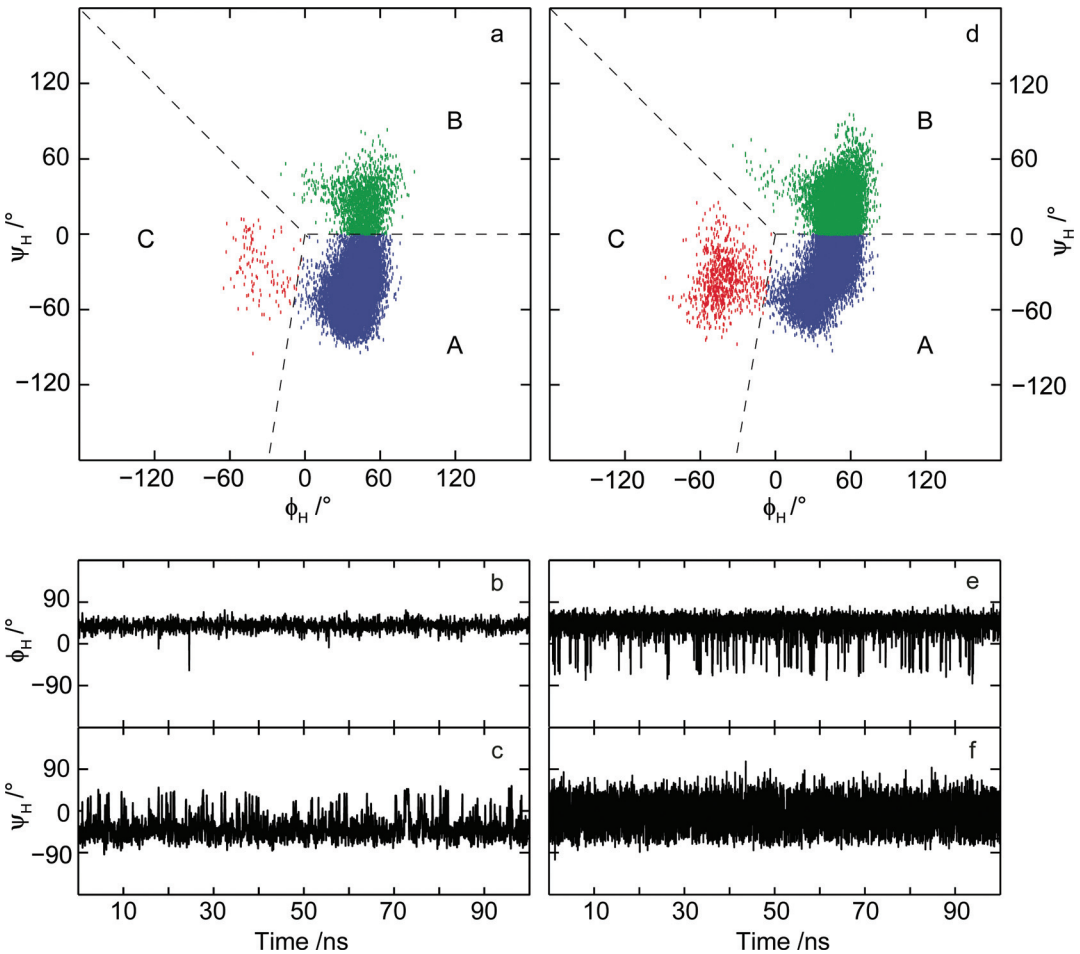

Fig. 7 Scatter plots and time dependence of the glycosidic torsion angels ϕ_H and ψ_H in α-L-Rha*p*-(1 → 2)-α-L-Rha*p*-OMe (a–c) and in α-L-Rha*p*-(1 → 3)-α-L-Rha*p*-OMe (d–f) from the MD simulations using the PARM22/SU01 force field. The conformational space is divided into three regions denoted A, B and C.

residual dipolar couplings are measured and utilized in the conformational analysis.[50]

For interpretation of the experimentally derived NMR data in a conformational model an MD simulation of R2R was carried out with explicit water molecules as solvent. The simulation closely mirrors the information that can be concluded from the Ramachandran map, *i.e.*, the major conformational state is present for the A-region, and the minor one occurs for the B-region; the third conformational state is hardly populated (Fig. 7a). A large number of transitions between conformations A and B occurs during the 100 ns simulation; thus, this region of conformational space is well sampled (Fig. 7b and 7c). The extent to which the three regions are populated is for A: 90%, B: 9%, and C: 1%. The average conformation given by the glycosidic torsion angles in R2R was $\phi_H = 39°$ and $\psi_H = -38°$, shown in Fig. 8.

From MD trajectories effective proton–proton distances can be calculated and indirect spin–spin coupling constants predicted

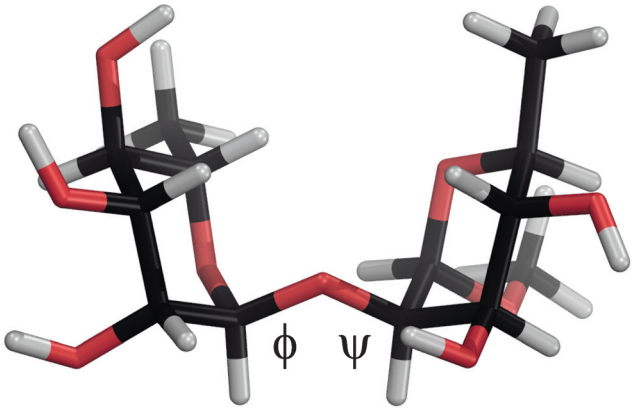

Fig. 8 Molecular model of R2R with glycosidic torsion angles ϕ_H = 39°and ψ_H = −38° (average conformation from the MD simulation).

using pertinent Karplus-type relationships. The four interresidue proton–proton distances obtained from the present MD simulation were compared to those previously determined by ^{1}H,^{1}H-T-ROESY NMR experiments:[30] H1′,H2 was 2.28 Å in the MD simulation *vs.* 2.24 Å from experiment; H1′,H1 was 2.84 *vs.* 3.10 Å; H5′,H1 was 2.70 *vs.* 2.59 Å; H2′,H2 was 3.81 *vs.* 3.99 Å. Thus, for effective proton–proton distances the agreement between simulation and experiment is indeed good. However, in order to attain concordance between the two, small changes to the force field would be needed such as a shift of the average torsion angle ψ_H towards a less negative value. The MD simulation of R2R may also be used to calculate $^nJ_{CH}$ coupling constants *via* Karplus-type relationships where averaging is carried out over all saved conformations, *i.e.*, 5 × 10^5 coordinate sets over the 100 ns of simulation. The agreement between computed $^nJ_{CH}$ coupling constants and experimentally determined ones, using a novel set of Karplus-type relationships[51] denoted JCX/SU09, is good for the ^3J-couplings related to the ϕ torsion angle whereas those related to the ψ torsion angle still deviate (Table 3); future force field improvements will probably remedy the remaining differences, in particular since there are now accurate experimental data to compare to, besides the recently developed Karplus-type relationships for both $^3J_{CH}$ and $^3J_{CC}$ coupling constants.

With the detailed information obtained for R2R we decided to extend the study to larger structures with the aim of shedding light on the 3D structures of larger oligosaccharides and polysaccharides. Another common disaccharide structural component of bacterial polysaccharides is α-L-Rha*p*-(1 → 3)-α-L-Rha*p* and a corresponding 100 ns MD simulation was also carried out for the methyl glycoside of this disaccharide, *i.e.*, α-L-Rha*p*-(1 → 3)-α-L-Rha*p*-OMe (R3R); the scatter plot and glycosidic torsion angle trajectories are shown in Fig. 7d–7f. Again the conformational states denoted A, B and C are present (Fig. 7d), but the populations in the conformational equilibrium are now compared to R2R changed to 53 : 43 : 4, respectively, *i.e.*, the two major conformational states are approximately equally populated. The plausibility of this population distribution was verified by computing the transglycosidic $^3J_{CH}$ coupling constants over the 100 ns simulation using the JCX/SU09 implementation leading to $^3J_{H1',C3}$ = 3.7 Hz and $^3J_{C1',H3}$ = 4.7 Hz for the couplings related to the ϕ_H and ψ_H torsion angles, respectively. These coupling constants were compared to those determined previously using the 1DLR experiment, *viz.*, 4.1 and 5.1 Hz, respectively.[29] The excellent agreement between the two computed and the experimentally determined $^3J_{CH}$ coupling constants leads credence to the population distribution described. Thus, the α-(1 → 3)-linkage should be regarded as flexible with two significantly and close to equally populated conformational states, as well as some population of a non-*exo*-anomeric conformation (conformation C), at the disaccharide level of complexity.

Some time ago rhamnan oligosaccharides related to the *O*-antigen polysaccharide isolated from *Pseudomonas syringae* pvs. coronafaciens IMV 9030[52] were synthesized and their conformational preferences investigated by NMR spectroscopy and molecular modeling as well as MD simulations.[53] The tri-, hexa-, and nonasaccharides corresponding to the repeating unit →3)-α-L-Rha*p*-(1 → 3)-α-L-Rha*p*-(1 → 2)-α-L-Rha*p*-(1→ investigated by NMR NOEs were concluded to populate the conformational states with a positive ψ torsion angle most of the time for both the α-(1 → 2)- and α-(1 → 3)-linkages as deduced by molecular modeling and the Ramachandran maps revealing regions of low potential energy. Predicted NOEs using a full matrix relaxation approach for the conformations deduced by molecular modeling and MD simulations were found to be in good agreement with those determined experimentally. These comprise *e.g.* for the α-L-Rha*p*-(1 → 2)-α-L-Rha*p* structural component the dipolar interactions between H1′ and H2 as well as H5′ and H1 interproton pairs. Consequently, the molecular modeling and MD simulations were judged reliable. However, these two proton pairs' effective distances in the disaccharide are equally well described by a conformation with a negative ψ torsion angle,[27] and it has been shown that the major conformational state of R2R is that in which the ψ torsion angle takes a negative value.[30] In order to differentiate between these two conformations, *i.e.*, with a positive or a negative ψ torsion angle (cf. Fig. 7a, regions B and A, respectively) one has to *e.g.* acquire information on the effective ^{1}H,^{1}H-distances between H1′ and H1 or H2′ and H2 which will reveal which of the two conformational states that is the preferred one or indicate the relative populations if there is a conformational equilibrium skewed towards one of them, in a corresponding way to the analysis performed for α-D-Man*p*-(1 → 2)-α-D-Man*p*-(1 → *O*)-L-Ser.[54]

To investigate whether the intrinsic conformational populations at the α-(1 → 2)- and α-(1 → 3)-linkages were present also for larger oligosaccharides we performed additionally an MD simulation on a hexasaccharide with the use of explicit water molecules. The structure of the hexasaccharide is shown in Fig. 1. Analysis of the 100 ns MD simulation revealed that only small conformational and population changes occurred (Fig. 9) and this is summarized in Table 3 for torsion angles and heteronuclear three-bond coupling constants compared to the disaccharide constituents. A shift in the average conformations occurs for some ψ torsion angles as a result of slightly larger populations of conformational states denoted B, having a positive ψ torsion angle. Again some population of a non-*exo*-anomeric conformation C is present at both the α-(1 → 2)- and α-(1 → 3)-linkages.

The conformational preferences of the disaccharides and the proposed torsion angle equilibria in the hexasaccharide can now

Table 3 Torsion angles, coupling constants (calculated with JCX/SU09) and distributions between the three states (A, B and C) from the 100 ns simulations

				MD hexasaccharide			MD disaccharide			$\Delta_{hexa-di}$		
Linkage	Distribution/%	Torsion angle		Torsion (°)	$J_{C,H}$ (Hz)	$^3J_{C,C}$ (Hz)	Torsion (°)	$J_{C,H}$ (Hz)	$^3J_{C,C}$ (Hz)	Torsion (°)	$J_{C,X}$ (Hz)	
II → I	A 72 (90)[a]	ϕ_H	H1′–C1′–O2 –C2	41 (15)	4.0		39 (12)	4.3		2	−0.3	ϕ_H
α-L-Rha*p*-(1 →	B 26 (9)	ψ_H	C1′–O2 –C2 –H2	–23 (34)	3.8		–38 (26)	3.4		15	0.4	ψ_H
2)-α-L-Rha*p*	C 2 (1)	$\phi_{C2'}$	C2′–C1′–O2 –C2	161 (14)		4.0[b]	158 (11)		4.0[b]	3	0.0	$\phi_{C2'}$
		ψ_{C1}	C1′ –O2 –C2 –C1	98 (33)		1.5[b]	84 (25)		1.2[b]	14	0.3	ψ_{C1}
		ψ_{C3}	C1′–O2 –C2 –C3	–144 (32)		2.6	–157 (25)		3.2	13	−0.6	ψ_{C3}
		$\phi_{O5'}$	O5′–C1′–O2 –C2	−79 (15)			–80 (12)					$\phi_{O5'}$
III → II	A 48 (53)	ϕ_H	H1′–C1′–O3 –C3	44 (18)	3.7		41 (21)	3.7		3	0.0	ϕ_H
α-L-Rha*p*-(1 →	B 49 (43)	ψ_H	C1′–O3 –C3 –H3	0 (26)	5.2		–7 (32)	4.7		7	0.5	ψ_H
3)-α-L-Rha*p*	C 3 (4)	$\phi_{C2'}$	C2′–C1′–O3 –C3	163 (17)		4.0[b]	160 (21)		3.9[b]	3	0.1	$\phi_{C2'}$
		ψ_{C2}	C1′ –O3 –C3 –C2	118(25)		1.2	112 (30)		1.2	6	0.0	ψ_{C2}
		ψ_{C4}	C1′–O3 –C3 –C4	−122 (24)		1.4	–128 (30)		1.8	6	−0.4	ψ_{C4}
		$\phi_{O5'}$	O5′–C1′–O3 –C3	−76 (24)			–78 (21)					$\phi_{O5'}$
IV → III	A 35	ϕ_H	H1′–C1′–O3 –C3	44 (20)	3.6					3	−0.1	ϕ_H
α-L-Rha*p*-(1 →	B 62	ψ_H	C1′–O3 –C3 –H3	8 (27)	5.0					15	0.3	ψ_H
3)-α-L-Rha*p*	C 3	$\phi_{C2'}$	C2′–C1′–O3 –C3	163(19)		4.0[b]				3	0.1	$\phi_{C2'}$
		ψ_{C2}	C1′ –O3 –C3 –C2	126 (26)		1.6				14	0.4	ψ_{C2}
		ψ_{C4}	C1′–O3 –C3 –C4	–115 (25)		1.1				13	−0.7	ψ_{C4}
		$\phi_{O5'}$	O5′–C1′–O3 –C3	−75 (19)								$\phi_{O5'}$
V → IV	A 72	ϕ_H	H1′–C1′–O2 –C2	42 (15)	4.0					3	−0.3	ϕ_H
α-L-Rha*p*-(1 →	B 26	ψ_H	C1′–O2 –C2 –H2	–22 (32)	4.0					16	0.6	ψ_H
2)-α-L-Rha*p*	C 2	$\phi_{C2'}$	C2′–C1′–O2 –C2	161 (14)		4.0[b]				3	0.0	$\phi_{C2'}$
		ψ_{C1}	C1′ –O2 –C2 –C1	99 (30)		1.4[b]				15	0.2	ψ_{C1}
		ψ_{C3}	C1′–O2 –C2 –C3	–142 (30)		2.5				15	−0.7	ψ_{C3}
		$\phi_{O5'}$	O5′–C1′–O2 –C2	−79 (15)								$\phi_{O5'}$
VI → V	A 48	ϕ_H	H1′–C1′–O3 –C3	41 (22)	3.7					0	0.0	ϕ_H
α-L-Rha*p*-(1 →	B 47	ψ_H	C1′–O3 –C3 –H3	–2 (27)	5.1					5	0.4	ψ_H
3)-α-L-Rha*p*	C 5	$\phi_{C2'}$	C2′–C1′–O3 –C3	160 (21)		3.9[b]				0	0.0	$\phi_{C2'}$
		ψ_{C2}	C1′ –O3 –C3 –C2	117 (26)		1.2				5	0.0	ψ_{C2}
		ψ_{C4}	C1′–O3 –C3 –C4	–124 (25)		1.5				4	−0.3	ψ_{C4}
		$\phi_{O5'}$	O5′–C1′–O3 –C3	−78 (21)								$\phi_{O5'}$

[a] Distributions between the three states in the disaccharides are given in parentheses. [b] With constant in-plane effect.

be utilized to predict the 3D structure of shape of larger oligosaccharides and subsequently polysaccharides. For a nonasaccharide [→ 3)-α-L-Rha*p*-(1 → 3)-α-L-Rha*p*-(1 → 2)-α-L-Rha*p*-(1 →]$_3$ having ψ torsion angles corresponding to all-A conformations may be contrasted to the one with all-B conformations (Fig. 10). The all-B structure is conspicuously more extended. The herein described all-B structure is similar to that previously reported;[53] however, based on the results presented above in this study neither the all-A nor the all-B conformations for the nonasaccharide are populated to any significant extent. The 3D structure should therefore be represented at each glycosidic linkage by a conformational equilibrium of two significantly populated conformations having either a positive or a negative value at the ψ torsion angles. Thus, the description of the canonical all-A and all-B structures of the nonasaccharide may be useful for visualization, but its 3D structure is dynamic in between the idealized all-A and all-B conformations.

In conclusion, synthesis of ^{13}C site-specific labeling in R2R has facilitated the extraction of both $^nJ_{CH}$ and $^nJ_{CC}$ coupling constants by 1D and 2D NMR experiments as well as by total line-shape analysis. Coupling constants having torsion angle dependences were used in the conformational analysis of the disaccharide. For the disaccharide the fourteen hitherto experimentally determined NMR parameters in isotropic solution correspond to an unusually large number of conformationally dependent data. The MD simulation of R2R, in conjunction with experimental NMR data, indicates a major conformational state having the most probable conformation at $\phi_H \approx 40°$ and $\psi_H \approx -35°$. The knowledge of conformational preferences and accessible conformational states of disaccharide models facilitate analysis of larger oligosaccharides and polysaccharides containing L-rhamnose residues, such as the nonasaccharide presented which is proposed to exist as a quite flexible oligosaccharide since a conformational equilibrium at each ψ torsion angle is

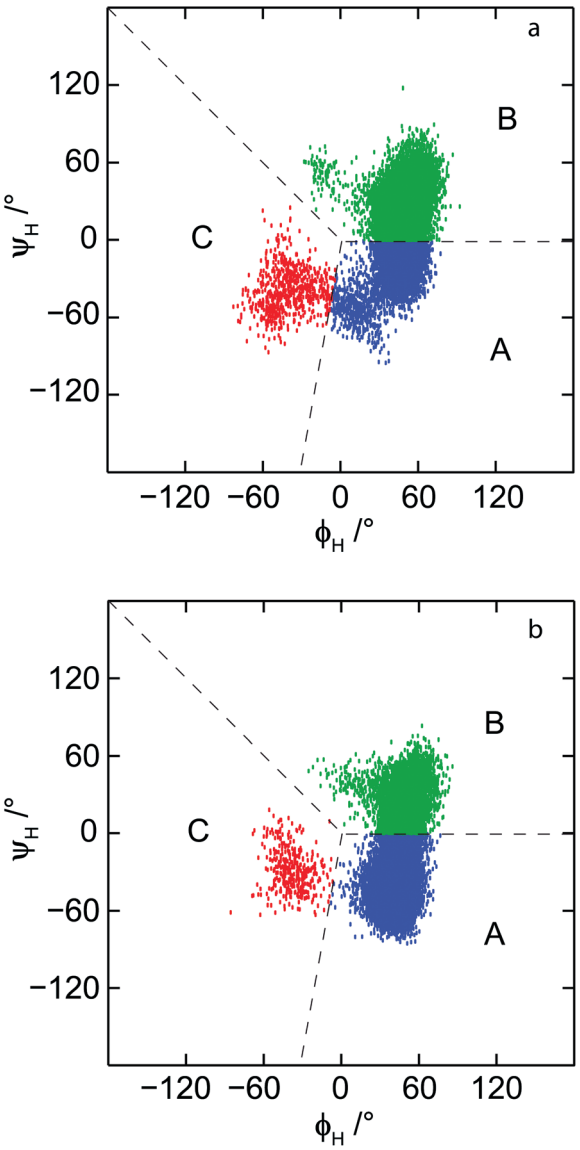

Fig. 9 Representative scatter plots of the glycosidic torsion angels ϕ_H and ψ_H in the hexasaccharide; (a) between residues IV and III, in an α-(1 → 3)-linkage, and (b) between residues V and IV, in an α-(1 → 2)-linkage.

present leading to a dynamic 3D structure where the bounds are the canonical all-A and all-B conformations.

Materials and methods

General

The site-specifically ^{13}C-labeled starting materials, L-[1-^{13}C] rhamnose and L-[2-^{13}C]rhamnose, both 99 atom% ^{13}C, were purchased from OMICRON Biochemicals, Inc., USA. TLC analysis was performed on precoated Merck 60 F_{254} plates and developed with 8% H_2SO_4. Solvents specified as dry were stored over molecular sieves and used without further purification. In the glycosylation reactions dichloromethane from Fluka (puriss, absolute, kept over molecular sieves) was used to avoid contamination from ethanol. For purification *via* column chromatography

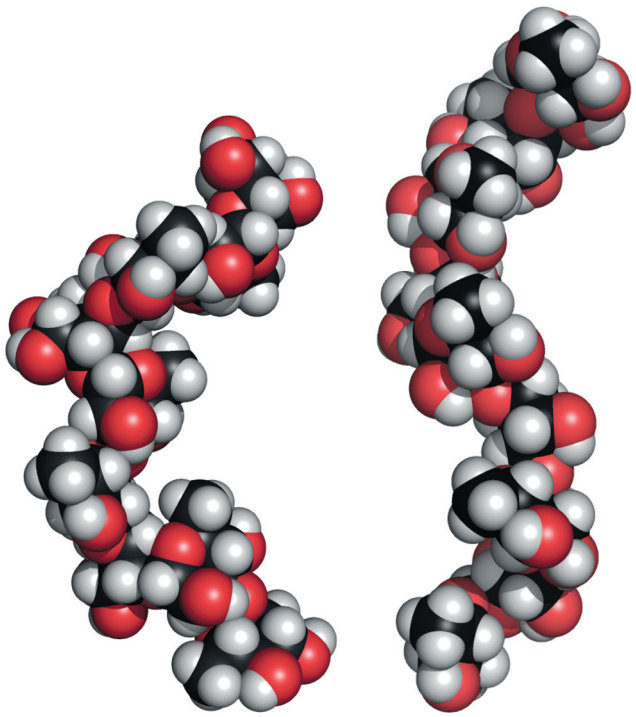

Fig. 10 Space-filling representation of the rhamnan nonasaccharide [→ 3)-α-L-Rha*p*-(1 → 3)-α-L-Rha*p*-(1 → 2)-α-L-Rha*p*-(1 →]$_3$ in the all-A (left) and the all-B (right) conformations.

Davisil silica medium (35–70 micron) was used. NMR spectroscopy was performed on Varian 400 MHz or Bruker AVANCE 500 MHz spectrometers at ambient temperature except otherwise stated. The ^{1}H and ^{13}C chemical shifts are referenced to the solvent $CDCl_3$ (δ_H 7.26, δ_C 77.23) or external TSP in D_2O (δ_H 0.00) and external dioxane in D_2O (δ_C 67.4) for D_2O-solutions. High-resolution mass spectrometry analysis was performed on a Bruker Daltonics ESI-TOF spectrometer in the positive mode. The detailed synthesis procedures are described for non-labeled materials; the ^{13}C-labeled compounds were obtained under the same conditions.

Glycosidic torsion angles are defined as follows: ϕ = O5′–C1′–On–Cn, ϕ_H = H1′–C1′–On–Cn, $\phi_{C2'}$ = C2′–C1′–On–Cn, ψ = C1′–On–Cn–C(n−1), ψ_H = C1′–On–Cn–Hn, ψ_{C3} = C1′–O2–C2–C3, and ψ_{C4} = C1′–O3–C3–C4, where n is the substitution position and atoms in the non-reducing end residue of the glycosidic linkage are denoted by a prime. The regions of conformational space spanning $-180° < \phi_H < 180°$ and $-180° < \psi_H < 180°$ are defined by the following states, A: $\psi_H < 0°$ and $\psi_H < 6\phi_H$; B: $\psi_H > 0°$ and $\psi_H > -\phi_H$; C: $\phi_H < 0°$ and $\psi_H < -\phi_H$ and $\psi_H > 6\phi_H$.

Experimental

2,3,4-Tri-*O*-benzoyl-α-L-rhamnopyranosyl bromide (2)

L-Rhamnose (254 mg, 1.4 mmol) was dissolved in dry pyridine (20 mL) and benzoyl chloride (1.0 mL, 6 eq.) was added at 0 °C. The solution was stirred at 60 °C for 5 h and monitored by TLC (Toluene : Ethyl acetate (T : E) 4 : 1). When complete, the reaction mixture was allowed to attain r.t.; water (0.2 mL) was

added and after 15 min the mixture was diluted with CH_2Cl_2. The organic phase was washed with cold water, H_2SO_4 (1 M), sat. $NaHCO_3$ (aq.) and then water again. The organic phase was dried over $MgSO_4$, the solvent was evaporated under reduced pressure and subsequently co-evaporated four times with toluene. The obtained yellow amorphous material (750 mg, 1.3 mmol) was dissolved in 10 mL glacial HOAc at r.t. To the solution was added 6 mL HBr in HOAc (12 mM) and the mixture was stirred at r.t. When the reaction, monitored by TLC (T : E 6 : 1), was complete after 6 h, ice and CH_2Cl_2 was added and the organic phase was washed with ice/water, sat. $NaHCO_3$ (aq.) and subsequently water. The organic solution was dried over Na_2SO_4 and subsequently concentrated under reduced pressure. Compound **2** was obtained in 84% yield (647 mg, 1.2 mmol). ^{1}H NMR (selected resonance, $CDCl_3$) δ: 6.20 (H1); ^{13}C NMR ($CDCl_3$) δ: 17.4 (Me), 69.1–73.6 (C2–C5), 84.0 (C1), 128.6–134.0 (aromatic C), 165.4–165.9 (3 × CO).

Methyl 3,4-di-*O*-benzoyl-α-L-rhamnopyranoside (3)

A solution of methyl 4-*O*-benzoyl-2,3-*O*-isopropylidene-α-L-rhamnopyranoside (1.1 g, 3.4 mmol) in acetic acid (40 mL, 70% aq.) was heated to 80 °C. After 2.5 h, the mixture was allowed to attain r.t., the solvent was evaporated and the resulting mixture co-evaporated three times with toluene. The oily residue was dissolved in a mixture of dry pyridine and dry CH_2Cl_2 (1 : 2) and cooled to −40 °C on a dry ice–acetone bath. Benzoyl chloride (0.35 mL, 1 eq.) was dissolved in dry pyridine : dry CH_2Cl_2 (1 : 2) and added dropwise to the mixture. The solution was then stirred at r.t. for 1 h, monitored by TLC (T : E 2 : 1), after which water was added. The mixture was diluted with CH_2Cl_2 and the organic phase washed with cold water, H_2SO_4 (1 M), sat. $NaHCO_3$ (aq.) and then water again. The organic phase was dried over Na_2SO_4 and the solvent was evaporated. The crude material was purified by flash chromatography on a column of silica (gradient, T → T : E 4 : 1). Compound **3** was obtained in 69% yield (889 mg, 2.3 mmol). ESI-MS: *m/z* $[M + Na]^+$ 409.127, expected 409.126. ^{1}H NMR (selected resonance, $CDCl_3$) δ: 4.80 (H1, $J_{H1,H2}$ 1.8 Hz); ^{13}C NMR ($CDCl_3$) δ: 17.8 (Me), 55.4 (OMe), 66.6–72.8 (C2–C5), 100.8 (C1), 128.6–133.5 (aromatic C), 165.8–166.0 (2 × CO).

Methyl 3,4-di-*O*-benzoyl-2-*O*-(2,3,4-tri-*O*-benzoyl-α-L-rhamnopyranosyl)-α-L-rhamnopyranoside (4)

A flask with **2** (245 mg, 0.45 mmol), **3** (275 mg, 1.6 eq.) and molecular sieves (4 Å) was placed under vacuum over night. The solids were dissolved in dry CH_2Cl_2, *sym*-collidine (approx. 50 mg, 1 eq.) was added and the suspension stirred at r.t. for 15 min under argon atmosphere. The mixture was cooled to −40 °C and AgOTf (125 mg, 1.1 eq.) was added in one portion. The mixture was stirred for 2 h and monitored by TLC (T : E 10 : 1) during which the temperature was allowed to rise to r.t. and pyridine was added to quench the reaction. The mixture was filtered through a pad of Celite and subsequently concentrated under reduced pressure. The crude material was purified on a column of silica (gradient, T → T : E 30 : 1). Compound **4** was obtained in 82% yield (311 mg, 0.37 mmol). ^{1}H NMR (selected resonances, $CDCl_3$) δ: 1.36 (H6′), 1.41 (H6), 4.12 (H5), 4.31 (H2), 4.34 (H5′), 4.90 (H1, $J_{H1,H2}$ 1.8 Hz), 5.16 (H1′, $J_{H1',H2'}$ 1.8 Hz), 5.66 (2H, H4, H4′), 5.79 (H3), 5.86 (H2′), 5.97 (H3′), 7.2–8.1 (25H, aromatic H); ^{13}C NMR ($CDCl_3$) δ: 17.9 (2C, C6, C6′), 55.4 (OMe), 67.0 (C5), 67.8 (C5′), 69.9 (C3′), 70.8 (C2′), 71.3 (C3), 72.0 (2C, C4, C4′), 76.8 (C2), 99.7 (C1′), 100.0 (C1), 128.4–133.6 (aromatic C), 165.3–166.1 (5 × CO).

Methyl 2-*O*-α-L-rhamnopyranosyl-α-L-rhamnopyranoside (1)

Compound **4** (176 mg, 0.21 mmol) was dissolved in NaOMe–MeOH (15 mL, 0.1 M) and the solution was stirred at r.t. for 2.5 h. The reaction was monitored by TLC (E : MeOH : H_2O 7 : 2 : 1). To neutralize, Dowex-50 (H^+-form) was added until the pH stabilized to approx. 7. The solution was filtered through a glass filter funnel, then passed through a short plug of Bio-Gel P-2 and freeze-dried. The crude material was purified on a column of Bio-Gel P-2 using water containing 1% *n*-butanol as eluent. Compound **1** was obtained in 79% yield (54 mg, 0.17 mmol) after lyophilization. ^{1}H and ^{13}C NMR spectral data were in agreement with those previously published.[38]

α-L-[1′-^{13}C]Rha*p*-(1 → 2)-α-L-Rha*p*-OMe (1-*c*1′)

Yield 60% (over 3 steps). ESI-MS: *m/z* $[M + Na]^+$ 348.1338, expected 348.1346. ^{1}H NMR (selected resonance, D_2O, 37 °C) δ: 4.96 (H1′, $J_{H1',H2'}$ 1.8 Hz, $J_{H1',C1'}$ 170 Hz).

α-L-[2′-^{13}C]Rha*p*-(1 → 2)-α-L-Rha*p*-OMe (1-*c*2′)

Yield 66% (over 3 steps). ESI-MS: *m/z* $[M + Na]^+$ 348.1350, expected 348.1346 ^{1}H NMR (selected resonance, D_2O, 37 °C) δ: 4.96 (H1′, $J_{H1',H2'}$ 1.8 Hz).

NMR spectroscopy

NMR samples of α-L-Rhap-(1 → 2)-α-L-Rhap-OMe (**1**), α-L-[1′-^{13}C]Rhap-(1 → 2)-α-L-Rhap-OMe (**1-*c*1′**) and α-L-[2′-^{13}C]Rhap-(1 → 2)-α-L-Rhap-OMe (**1-*c*2′**) were prepared in D_2O (pD 6) to concentrations of <100 mM. NMR experiments were recorded at 37 °C on Bruker AVANCE 500 MHz and Bruker AVANCE III 700 MHz spectrometers; both equipped with 5 mm TCI Z-Gradient CryoProbes. The chemical shifts are referenced to external sodium 3-trimethylsilyl-(2,2,3,3-$^2H_4$)-propanoate (TSP) in D_2O (δ_H 0.00) and external dioxane in D_2O (δ_C 67.4). The ^{13}C NMR experiments were recorded over 109.2 ppm with 76′920 points and the FIDs zero-filled to 2048k data points. To measure ^{13}C,^{13}C coupling constants a Lorentz–Gaussian window function (lb = −0.5 to −1.5, gb = 0.5) was applied. The ^{1}H,^{13}C-HSQC-HECADE experiment[44] was recorded with 160 scans per t_1-increment, a DIPSI-2 spin-lock and a mixing time of 30 ms. A 2D matrix of 256 × 2k data points in F_1 and F_2 dimensions, respectively, a t_1^*/t_1 scaling factor of unity and the echo-antiecho method were used. Prior to Fourier transformation zero-filling was carried out to 4k × 8k data points and 90° shifted squared sine-bell functions were applied in both dimensions. For compound **1** the ^{1}H,^{13}C-J-HMBC NMR experiments[45] were recorded as described[55,56] using five different values of the

scaling factor κ between 10 and 34. ^{1}H NMR chemical shifts and ^{n}J coupling constants were refined from 1D spectra using the PERCH NMR software (PERCH Solutions Ltd., Kuopio, Finland).

Computer simulations

For the molecular dynamics (MD) simulations CHARMM[57] software was used employing a CHARMM22 type of force field modified for carbohydrates and referred to as PARM22/SU01.[37] Initial conditions were prepared by placing each disaccharide in a cubic water box of length 29.97 Å containing 900 modified TIP3P water molecules.[58] The hexasaccharide was placed in a water box of length 50 Å containing 3921 modified TIP3P water molecules. The solvent molecules that were closer than 2.5 Å to any solute atom were removed resulting in 868 water molecules for R2R, 864 water molecules for R3R, and 3838 water molecules for the hexasaccharide. Energy minimization was performed with Steepest Descent, 200 steps, followed by Adopted Basis Newton–Raphson until the root-mean-square gradient was less than 0.01 kcal·mol^{-1}·Å^{-1}. The initial velocities were assigned at 105 K, followed by heating with 5 K increments during 8 ps to 310 K, where the systems were equilibrated for 1 ns. The production runs were performed for 100 ns at 310 K. Simulations were carried out at the Center for Parallel Computers, KTH, Stockholm, using 1 node with two quad-core processors per node. For the disaccharides parallel version C34b2 was used and for the hexasaccharide version C35b4 was used. The CPU time was approximately 2.5 h per ns for the disaccharides and 6.5 h per ns for the hexasaccharide.

The potential energy maps were computed from a 15° grid search over the entire glycosidic torsion angle space using a dielectric constant of 3. Energy minimization was performed with Steepest Descent, 50 steps, followed by Adopted Basis Newton–Raphson until the root-mean-square gradient was less than 0.01 kcal·mol^{-1}·Å^{-1}. The nonasaccharide was built by CarbBuilder[59] as part of CASPER[60] and visualization of oligosaccharides was made using PyMOL (The PyMOL Molecular Graphics System, Version 0.99rc6, Schrödinger, LLC).

Acknowledgements

This work was supported by grants from the Swedish Research Council (VR), The Knut and Alice Wallenberg Foundation, and Carl Tryggers Stiftelse för Vetenskaplig Forskning. The Center for Parallel Computers (PDC), Stockholm, Sweden, is thanked for computing resources.

References

1 *Essentials of Glycobiology* ed. A. Varki, R. Cummings, J. Esko, H. Freeze, G. Hart and J. Marth, Cold Spring Harbor Laboratory Press, Cold Spring Harbor, 1999.
2 B. Lindberg, in *Polysaccharides* ed. S. Dumitriu, Marcel Dekker, New York, 1998, pp. 237–273.
3 N. I. A. Carlin and T. Wehler, *Eur. J. Biochem.*, 1988, **176**, 471–476.
4 J. Kulber-Kielb, E. Vinogradov, C. Chu and R. Schneerson, *Carbohydr. Res.*, 2007, **342**, 643–647.
5 M. Ansaruzzaman, M. J. Albert, T. Holme, P.-E. Jansson, M. M. Rahman and G. Widmalm, *Eur. J. Biochem.*, 1996, **237**, 786–791.
6 K. Steiner, R. Novotny, D. B. Werz, K. Zarschler, P. H. Seeberger, A. Hofinger, P. Kosma, C. Schäffer and P. Messner, *J. Biol. Chem.*, 2008, **283**, 21120–21133.
7 A. Turska-Szewczuk, A. Kozinska, R. Russa and O. Holst, *Carbohydr. Res.*, 2010, **345**, 680–684.
8 A. Molinaro, M.-A. Newman, R. Lanzetta and M. Parrilli, *Eur. J. Org. Chem.*, 2009, 5887–5896.
9 P.-E. Jansson, L. Kenne and T. Wehler, *Carbohydr. Res.*, 1987, **166**, 271–282.
10 J.-R. Brisson, H. Baumann, A. Imberty, S. Pérez and H. J. Jennings, *Biochemistry*, 1992, **31**, 4996–5004.
11 M. Michela Corsaro, C. De Castro, T. Naldi, M. Parrilli, J. M. Tomás and M. Regué, *Carbohydr. Res.*, 2005, **340**, 2212–2217.
12 I. Sánchez-Medina, M. Frank, C.-W. von der Lieth and J. P. Kamerling, *Org. Biomol. Chem.*, 2009, **7**, 280–287.
13 B. Coxon, N. Sari, G. Batta and V. Pozsgay, *Carbohydr. Res.*, 2000, **324**, 53–65.
14 M.-J. Clément, A. Imberty, A. Phalipon, S. Pérez, C. Simenel, L. A. Mulard and M. Delepierre, *J. Biol. Chem.*, 2003, **278**, 47928–47936.
15 V. Pozsgay, N. Sari and B. Coxon, *Carbohydr. Res.*, 1998, **308**, 229–238.
16 G. Batta and A. Lipták, *J. Chem. Soc., Chem. Commun.*, 1985, 368–370.
17 A. Bax and R. Freeman, *J. Am. Chem. Soc.*, 1982, **104**, 1099–1100.
18 C. Bauer, R. Freeman and S. Wimpers, *J. Magn. Reson.*, 1984, **58**, 526–532.
19 J.-M. Nuzillard and J.-M. Bernassau, *J. Magn. Reson., Ser. B*, 1994, **103**, 284–287.
20 L. Poppe, S. Sheng and H. van Halbeek, *J. Magn. Reson., Ser. A*, 1994, **111**, 104–107.
21 T. Nishida, G. Widmalm and P. Sándor, *Magn. Reson. Chem.*, 1995, **33**, 596–599.
22 R. T. Williamson, B. L. Márquez, W. H. Gerwick and K. E. Kövér, *Magn. Reson. Chem.*, 2000, **38**, 265–273.
23 T. Parella and J. Belloc, *J. Magn. Reson.*, 2001, **148**, 78–87.
24 R. T. Williamson, B. L. Marquez, W. H. Gerwick, G. E. Martin and V. V. Krishnamurthy, *Magn. Reson. Chem.*, 2001, **39**, 127–132.
25 D. Uhrín, *J. Magn. Reson.*, 2002, **159**, 145–150.
26 P. Vidal, N. Esturau, T. Parella and J. F. Espinosa, *J. Org. Chem.*, 2007, **72**, 3166–3170.
27 G. Widmalm, R. A. Byrd and W. Egan, *Carbohydr. Res.*, 1992, **229**, 195–211.
28 B. J. Hardy, W. Egan and G. Widmalm, *Int. J. Biol. Macromol.*, 1995, **17**, 149–160.
29 B. J. Hardy, S. Bystricky, P. Kovac and G. Widmalm, *Biopolymers*, 1997, **41**, 83–96.
30 C. Landersjö, B. Stevensson, R. Eklund, J. Östervall, P. Söderman, G. Widmalm and A. Maliniak, *J. Biomol. NMR*, 2006, **35**, 89–101.
31 P. Söderman, S. Oscarson and G. Widmalm, *Carbohydr. Res.*, 1998, **312**, 233–237.
32 R. K. Ness, G. F. Hewitt Jr. and C. S. Hudson, *J. Am. Chem. Soc.*, 1951, **73**, 296–300.
33 H. Rainer, H.-D. Scharf and J. Runsink, *Liebigs Ann. Chem.*, 1992, 103–107.
34 T. Norberg, S. Oscarson and M. Szöni, *Carbohydr. Res.*, 1986, **152**, 301–304.
35 P. J. Garegg and T. Norberg, *Acta Chem. Scand., Ser. B*, 1979, **33**, 116–118.
36 H. Thøgersen, R. U. Lemieux, K. Bock and B. Meyer, *Can. J. Chem.*, 1982, **60**, 44–57.
37 R. Eklund and G. Widmalm, *Carbohydr. Res.*, 2003, **338**, 393–398.
38 P.-E. Jansson, L. Kenne and G. Widmalm, *Acta Chem. Scand.*, 1991, **45**, 517–522.
39 T. Nishida, G. Widmalm and P. Sándor, *Magn. Reson. Chem.*, 1996, **34**, 377–382.
40 T. E. Klepach, I. Carmichael and A. S. Serianni, *J. Am. Chem. Soc.*, 2005, **127**, 9781–9793.
41 I. Carmichael and A. S. Serianni, *Carbohydr. Res.*, 1996, **280**, 177–186.
42 F. Cloran, I. Carmichael and A. S. Serianni, *J. Am. Chem. Soc.*, 2000, **122**, 396–397.
43 W. Koźmiński and D. Nanz, *J. Magn. Reson.*, 1997, **124**, 383–392.
44 W. Koźmiński and D. Nanz, *J. Magn. Reson.*, 2000, **142**, 294–299.
45 A. Meissner and O. W. Sørensen, *Magn. Reson. Chem.*, 2001, **39**, 49–52.
46 R. Laatikainen, M. Niemitz, U. Weber, J. Sundelin, T. Hassinen and J. Vepsäläinen, *J. Magn. Reson., Ser. A*, 1996, **120**, 1–10.

47 G. Widmalm, in *Comprehensive Glycoscience*, ed. J. P. Kamerling, Elsevier, Oxford, 2007, pp. 101–132.
48 I. Carmichael, D. M. Chipman, C. A. Podlasek and A. S. Serianni, *J. Am. Chem. Soc.*, 1993, **115**, 10863–10870.
49 I. Tvaroska and F. R. Taravel, *Carbohydr. Res.*, 1991, **221**, 83–94.
50 P. Berthault, D. Jeannerat, F. Camerel, F. A. Salgado, Y. Boulard, J.-C. P. Gabriel and H. Desvaux, *Carbohydr. Res.*, 2003, **338**, 1771–1785.
51 E. Säwén, T. Massad, C. Landersjö, P. Damberg and G. Widmalm, *Org. Biomol. Chem.*, 2010, **8**, 3684–3695.
52 E. L. Zdorovenko, G. V. Zatonsky, G. M. Zdorovenko, L. A. Pasichnyk, A. S. Shashkov and Y. A. Knirel, *Carbohydr. Res.*, 2001, **336**, 329–336.
53 E. Bedini, C. De Castro, G. Erbs, L. Mangoni, J. M. Dow, A.-M. Newman, M. Parrilli and C. Unverzagt, *J. Am. Chem. Soc.*, 2005, **127**, 2414–2416.
54 K. Lycknert, A. Helander, S. Oscarson, L. Kenne and G. Widmalm, *Carbohydr. Res.*, 2004, **339**, 1331–1338.
55 E. Säwén, M. U. Roslund, I. Cumpstey and G. Widmalm, *Carbohydr. Res.*, 2010, **345**, 984–993.
56 K. H. M. Jonsson, R. Pendrill and G. Widmalm, *Magn. Reson. Chem.*, 2011, **49**, 117–124.
57 B. R. Brooks, C. L. Brooks III, A. D. MacKerell Jr, L. Nilsson, R. J. Petrella, B. Roux, Y. Won, G. Archontis, C. Bartels, S. Boresch, A. Caflisch, L. Caves, Q. Cui, A. R. Dinner, M. Feig, S. Fischer, J. Gao, M. Hodoscek, W. Im, K. Kuczera, T. Lazaridis, J. Ma, V. Ovchinnikov, E. Paci, R. W. Pastor, C. B. Post, J. Z. Pu, M. Schaefer, B. Tidor, R. M. Venable, H. L. Woodcock, X. Wu, W. Yang, D. M. York and M. Karplus, *J. Comput. Chem.*, 2009, **30**, 1545–1614.
58 E. Neria, S. Fischer and M. Karplus, *J. Chem. Phys.*, 1996, **105**, 1902–1921.
59 M. Kuttel, Y. Mao, G. Widmalm and M. Lundborg, Proc. 7th IEEE Int. Conf. e-Science 2011, 395–402.
60 M. Lundborg and G. Widmalm, *Anal. Chem.*, 2011, **83**, 1514–1517.